



Isomer-resolved online analysis of organic aerosols using ion mobility mass spectrometry

Andre F. Schaum¹, Christopher M. Kenseth², Madison Rutherford^{1,3}, Harald Stark^{1,3,4}, Manjula R. Canagaratna⁴, Joost A. de Gouw^{1,3}, Jose L. Jimenez^{1,3}, Kelvin H. Bates⁵

5 ¹Department of Chemistry, University of Colorado Boulder, Boulder, Colorado 80309, United States

²Department of Atmospheric and Oceanic Science, University of Maryland, College Park, Maryland 20742, United States

³Cooperative Institute for Research in the Environmental Sciences (CIRES), Boulder, Colorado 80309, United States

⁴Aerodyne Research Inc., Billerica, Massachusetts 01821, United States

⁵Department of Mechanical Engineering, University of Colorado Boulder, Boulder, Colorado 80309, United States

10 *Correspondence to:* Kelvin H. Bates (kelvin.bates@colorado.edu)

Abstract.

Secondary organic aerosol (SOA) makes up much of the particulate matter in the troposphere and impacts global climate and human health, though uncertainties regarding the sources and properties of SOA limit our understanding of these effects. New analytical techniques are required to better characterize the molecular composition of SOA, including methods that can identify isomeric compounds that may have different contributions to SOA properties such as hygroscopicity or volatility. We present a method for isomer-resolved analysis of SOA using a commercially available chemical ionization ion-mobility time-of-flight mass spectrometer (CI-IMS-TOF) and a Vaporization Inlet for Aerosols (VIA). The compatibility of the VIA and the CI-IMS-TOF was assessed through the analysis of 10 carboxylic acid standards across a large temperature range (30 - 170 °C). Ion drift times were found to be stable to within 0.075% of their initial values after drift time calibration. The VIA-CI-IMS-TOF was also used to collect real-time ion mobility and mass spectra of SOA constituents during an α -pinene ozonolysis chamber experiment. Several reaction products were identified in the SOA using synthetic standards, including structural isomers of C₈H₁₂O₄ and C₉H₁₄O₄. Temporal evolution of reaction products was used to assess formation timescales and determine the generation of oxidation for individual isomers. Both iodide and bromide reagent ions were used in the VIA-CI-IMS-TOF to achieve a more comprehensive analysis of SOA. This study demonstrates the performance of the VIA-CI-IMS-TOF for online, isomer-resolved analysis of organic aerosol and its potential for improving the current understanding of SOA composition.

1 Introduction

Much of the particulate matter in the troposphere consists of organic aerosol (OA), a major fraction of which can be attributed to secondary organic aerosol (SOA) formed through gas-phase oxidation of volatile organic compounds (VOCs; Zhang, 2007; Hallquist et al., 2009; Shrivastava et al., 2017). SOA influences global climate due to impacts on radiative forcing either



30 directly or through its role in cloud formation (as cloud condensation nuclei, CCN), though uncertainties in the magnitude of
this influence remain large (Shrivastava et al., 2017). One key to minimizing these uncertainties is a more comprehensive
understanding of the molecular composition of SOA, which enables more accurate predictions of physicochemical properties
such as hygroscopicity, volatility, and CCN activity (Pöschl, 2005). To achieve this better understanding, new analytical
techniques are required that can determine not only the chemical makeup of SOA constituents but also their molecular
structures. Isomers (both structural and stereoisomers) of organic compounds can exhibit substantial differences in properties
critical to aerosol modelling; for example, suberic acid (octanedioic acid) and dimethyl adipate (dimethyl hexanedioate) differ
35 in vapor pressure by approximately six orders of magnitude despite having the same molecular formula of $C_8H_{14}O_2$ (Verevkin
et al., 2006; Bilde et al., 2015). Thus, identifying just chemical formulas or molar masses within SOA is insufficient to
confidently infer important physicochemical properties, rendering the ability to separate isomeric species critical to improving
our current understanding of SOA on a molecular level and of its influence on global climate.

Numerous methods employing high-resolution mass spectrometry (HRMS) have been developed for isomer-resolved
analysis of SOA. Separation of isomers in SOA prior to HRMS detection is often achieved using liquid chromatography (LC)
paired with electrospray ionization (ESI; Hildmann and Hoffmann, 2024), though gas chromatography (GC) has also been
used. GC coupled with electron ionization with one-hour time resolution has been commercialized as the Thermal Desorption
45 Aerosol GC (TAG) instrument (Williams et al., 2006), which has since been paired with iodide CIMS for the separation of
standards and limonene-derived SOA (Bi et al. 2021a, b). Other heated inlets paired with chemical ionization mass
spectrometry (CIMS) have also been used. Among the most widely used is the Filter Inlet for Gases and AEROSols
(FIGAERO; Lopez-Hilfiker et al. 2014), which collects SOA on a Teflon filter and thermally desorbs particle-phase analytes
into a CIMS inlet. Isomer separation in the FIGAERO is based on volatility differences and achieves much lower resolution
50 than LC or GC. More recently, Schaum et al. (2025) coupled LC with I^- CIMS using an Aerodyne vaporization inlet for
aerosols (VIA) – an inlet consisting of a heated stainless steel tube with an inert coating – to measure SOA generated by α -
pinene ozonolysis as well as urban organic aerosol. These techniques are disadvantaged by their relatively long sampling and
separation timescales which, depending on the sample collection rate, can be on the order of tens of minutes to hours. Several
steps in offline sampling methods can also change the properties and species distribution of SOA through the loss of
55 semivolatile compounds from filters (Eatough et al., 2003), chemical transformations during storage (Resch et al., 2023), or
the generation of reactive oxygen species by ultrasonic irradiation (Miljevic et al., 2014). Additionally, separation by GC can
be challenging for low-volatility and thermally labile compounds, for which irreversible losses due to condensation or
decomposition can occur (Tobias and Ziemann, 2000). Although more amenable to low-volatility species, LC paired with ESI
is susceptible to matrix effects (Taylor, 2005; Amarandei et al., 2020) and ion suppression (Apffel et al., 1995; Law et al.,
60 2010) that can impact overall instrument sensitivity and make consistent quantification difficult.

As an alternative to chromatographic methods, ion mobility mass spectrometry (IM-MS) has also been employed on
several occasions for the separation of gas- and particle-phase isomers formed through VOC oxidation (Krechmer et al., 2016;
Zhang et al., 2017, 2019; West et al., 2023). Ion mobility spectrometry (IMS) separates gas-phase ions by their mobility



through a buffer gas (often helium or nitrogen) and, not being reliant on solvents or a stationary phase, does not suffer from
65 the same complications (*e.g.*, poor solubility, solvent incompatibilities) that can arise in GC and LC (Krechmer et al., 2016).
As demonstrated by Krechmer et al. (2016) and Skyttä et al. (2022), separation by ion mobility is compatible with a number
of different of ionization methods, including ESI and secondary electrospray ionization (SESI) with multiple reagent ions, as
well as nitrate (NO_3^-) CIMS. This was also shown recently by Chen et al. (2024), who used IMS coupled with a benzene CIMS
to separate and detect five different alkylammonium ions. These applications of IM-MS to atmospheric systems, however, are
70 exclusively offline methods for the measurement of aerosol species, with online analysis being limited to volatile and
semivolatile compounds in the gas phase. For example, Krechmer et al. (2016) and Skyttä et al. (2022) achieved online analysis
of gas-phase species with their respective methods, whereas offline analysis using filter sampling and ESI was required for
aerosol analysis by Krechmer et al. (2016), Zhang et al. (2019), and West et al. (2023). Another key advantage of IM-MS over
GC- or LC-based separations is the comparatively short sampling time scale, typically achieving separation of SOA
75 components in under 100 ms. This rapid separation allows IM-MS to be used in applications that require real-time monitoring
of reaction products such as environmental chamber experiments. However, at the time of writing, real-time measurements of
SOA using IM-MS have yet to be published, to our knowledge.

In this study, we present a technique for online, isomer-resolved analysis of SOA using an Aerodyne VIA coupled
with a commercially available chemical ionization ion-mobility time-of-flight mass spectrometer (CI-IMS-TOF). Using this
80 system, we achieve online separation of atmospherically relevant isomers in a way that isolates particle-phase species, avoids
the sampling and degradation issues associated with offline sampling and chromatography, and provides high enough time
resolution to monitor the evolution of an environmental chamber experiment. The compatibility of a heated inlet and IMS was
first determined through thermal ramping during analysis of organic acid standards. The ability of the system to separate and
detect isomers of organic compounds in SOA was evaluated through online analysis of the α -pinene ozonolysis reaction.
85 Synthetic reaction products were used to identify several structures. Finally, the use of both iodide and bromide CIMS reagent
ions to achieve a more comprehensive analysis of SOA using the VIA-CI-IMS-TOF of SOA is briefly discussed.

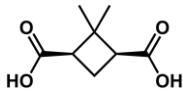
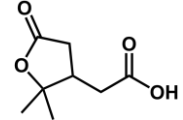
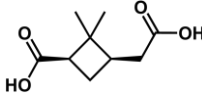
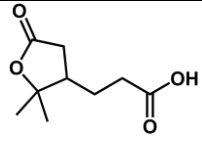
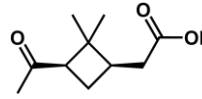
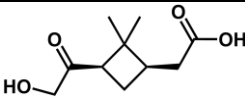
2 Materials and Methods

2.1 Chemicals

The following chemicals were used throughout the experiments described below: (1R)-(+)- α -pinene (99%, Sigma Aldrich),
90 ethyl acetate (ACS grade, EMD Millipore), adipic acid (99%, TCI America), pimelic acid (98%, Thermo Scientific), suberic
acid (99%, TCI America), azelaic acid (98%, Thermo Scientific), sebacic acid (98%, TCI America), undecanedioic acid (98%,
MedChemExpress), dodecanedioic acid (99%, TCI America), 2-hydroxypalmitic acid (97%, Ambeed, Inc.), 16-
hydroxypalmitic acid (98%, TCI America), and 12-hydroxystearic acid (95%, Thermo Scientific). Several α -pinene ozonolysis
products were synthesized previously (Kenseth et al., 2020, 2023, In Preparation) and used to identify compounds in the
95 chamber experiment (Table 1).



Table 1: Summary of synthesized α -pinene ozonolysis products.

Compound	Formula	Monoisotopic Mass (g/mol)	Structure	Reference
<i>cis</i> -norpinic acid	C ₈ H ₁₂ O ₄	172.0736		Kenseth et al. (In Preparation)
Terpenylic acid	C ₈ H ₁₂ O ₄	172.0736		Kenseth et al. (In Preparation)
<i>cis</i> -pinic acid	C ₉ H ₁₄ O ₄	186.0892		Kenseth et al. (2020, 2023)
Homoterpenylic acid	C ₉ H ₁₄ O ₄	186.0892		Kenseth et al. (In Preparation)
<i>cis</i> -pinonic acid	C ₁₀ H ₁₆ O ₃	184.1099		Kenseth et al. (2020)
<i>cis</i> -10-hydroxypinonic acid	C ₁₀ H ₁₆ O ₄	200.1049		Kenseth et al. (2023)

2.2 Instrumentation

100 The ToFwerk CI-IMS-TOF used here is described in more detail by Chen et al. (2024) and Rice et al. (2026). Ionization in the CI-IMS-TOF is achieved using a Vocus adduct ionization mechanism (AIM) ion molecule reactor described by Riva et al. (2024), which generates reagent ions by flowing dilute mixtures of reagent gases through a vacuum ultraviolet light source. The AIM reactor used in this study was held at 50 °C and the pressure was set at 50 mbar at the beginning of each experiment by manually adjusting a pressure control valve. The AIM was operated with either iodide (I⁻) or bromide (Br⁻) reagent ions generated from methyl iodide or dibromomethane, respectively. The ion drift region was filled with He at a pressure of 3.8 mbar with a tolerance of ±4 μbar. This pressure was regulated during instrument operation through automatic adjustments to the He flow. The traveling wave frequency was set to 49.528 kHz with a peak-to-peak amplitude of 21 V. An Aerodyne VIA was mounted orthogonally to the AIM inlet using a perfluoroalkoxy alkane (PFA) union tee. The VIA consists of a ~45 cm Sulfinert-coated stainless steel tube (0.64 cm outer diameter) insulated with glass wool. A honeycomb charcoal denuder

105



110 (Aerodyne Research Inc.) located immediately upstream of the VIA is used to remove gas-phase compounds from the sample
flow. The VIA can be heated up to 270 °C using a 24 V resistive heating element located under the insulation. A detailed
characterization of the VIA can be found elsewhere (Zhao et al., 2024). A vacuum line was also connected to the union (along
the VIA axis) to accelerate the sampling flow from the chamber through the VIA to 3 L min⁻¹, and the CI-IMS-TOF subsampled
1.8 L min⁻¹ from this flow. The VIA was held at 200 °C during the environmental chamber experiments discussed in Section
115 2.4.

The concentration of SOA formed during chamber experiments was measured using a scanning mobility particle sizer
(SMPS) consisting of a TSI model 3080 electrostatic classifier, 3081 differential mobility analyzer, and a 3776 condensation
particle counter. The SMPS was operated with a particle size range of 16 to 604 nm and aerosol size distributions were collected
every 135 s. A density of 1.2 g cm⁻³ was used to calculate aerosol mass concentration in the chamber (Shilling et al., 2009).

120 2.3 Data analysis

The VIA-CI-IMS-TOF data was stored in Tofwerk HDF data format and analyzed using the analysis software package
“Tofware” (Version 4.0.3.b64643; Stark et al., 2015) in Igor Pro 9 (WaveMetrics) with the added IMS analysis workflow. Due
to the large data volume present in IMS data files (4092 times more data compared to regular time-of-flight mass spectrometry
data), the analysis is divided into computationally intensive processing steps and user-interactive display steps.

125 In a first step, the user sets up time averaging and the peak list, which can contain both unit mass-resolution integration
regions and high resolution peaks. Then, the routine will extract 3-dimensional matrices with measurement time, peak number,
and drift time as the coordinates. A 2-dimensional image plot is generated that shows time vs. drift time for any peak from the
peaklist (Fig. S1). The user can then perform a peak fitting along the time dimension to retrieve time series for individual drift
time peaks within each mass spectral peak. Additionally, the drift time axis can be calibrated in two possible ways. Either, a
130 peak finding algorithm can be used to identify possible drift time calibration peaks that are persistent throughout the dataset
and isolated. This results in a somewhat arbitrary but internally consistent drift time axis which can vary from experiment to
experiment. Alternatively, to achieve more uniform drift times across multiple experiments, an initial set of drift time peaks
based on specific mass spectral peaks can be provided as the initialization point for the drift time calibration. The latter
procedure was employed in this work to be able to achieve better drift time positions from the same peaks during separate
135 experiments. Six fluorinated compounds that were consistently present in the background of each analysis (due to outgassing
from the Teflon permeation tubes and/or tubing) were used as calibrant ions for each experiment.

2.4 Analysis of Chemical Standards and Environmental Chamber Experiment

Experiments were conducted in a ~21 m³ Teflon chamber operated in batch mode (*i.e.*, without dilution or makeup clean air
flow) at ambient temperature (24-25 °C) and pressure (0.83 atm in Boulder, Colorado) (Krechmer et al., 2017). Two AADCO
140 clean air generators were used to fill the chamber with pure, dry air (<5 ppbv total hydrocarbons, ~0.1% RH). Standards and
VOCs were added to the chamber using a custom-built vaporizer (Finewax et al., 2020). Ozone was generated directly into the



chamber using pure O₂ (ultrahigh purity, Airgas) and a BMT 802N ozone generator, and the concentrations were verified using a Thermo Scientific Model 49i ozone analyzer. Aerosols were sampled from the environmental chamber through 2 m of conductive PFA (cPFA) tubing (Morris et al., 2024).

145 The first set of experiments involved the analysis of standards. Solutions of the seven dicarboxylic acid and three hydroxyacid standards were prepared in methanol at concentrations of 10 mM and 20 mM, respectively. Using the vaporizer, 40 µL of the dicarboxylic acid standard and 80 µL of the hydroxyacid standard were added to the chamber, where a fraction of the total mass condensed into aerosols. Each of the synthesized α -pinene ozonolysis products (5-10 mg) were dissolved in a minimal amount of ethyl acetate and small quantities (2-5 µL) were deposited onto Millipore Fluoropore PTFE filters (0.45
150 µm pore size). Using an in-line filter holder, the filters were placed between the VIA and the AIM reactor inlet, allowing heated chamber air to evaporate the standards and be carried into the instrument.

The second set of experiments involved the analysis of chamber SOA. One ozonolysis experiment was carried out for each of the two CI-IMS-TOF reagent ions (I⁻ and Br⁻). For each experiment, approximately 300 ppb of ozone was first added to the chamber. When the ozone concentration was stable (verified with the ozone monitor), 200 ppb of α -pinene was
155 added to the chamber on the order of several seconds with a Teflon-coated fan running throughout the injection to mix the chamber air. The fan was allowed to run for at least 15 s after the addition of α -pinene to allow for complete mixing of the chamber (Krechmer et al., 2016). The experiments were conducted without an OH scavenger, resulting in the production of OH radicals that also reacted with the α -pinene. Using a simple KinSim model (Peng and Jimenez, 2019) consisting of only first-generation reactions and an estimated OH yield from α -pinene ozonolysis of 80% (Presto and Donahue, 2004; Aschmann,
160 et al., 2002), it was estimated that approximately 56% of the α -pinene reacted with ozone and 44% reacted with OH. No seed aerosol was added to the chamber prior to the experiment, but nucleation and particle growth were observed within three minutes of the addition of α -pinene. During the ~80-minute experiment time, the ozone concentration decayed by 41% and a peak aerosol mass concentration of 370 µg m⁻³ (median particle size of 145 nm) was observed. The generated aerosol was measured continuously throughout the experiment.

165 **3 Results and Discussion**

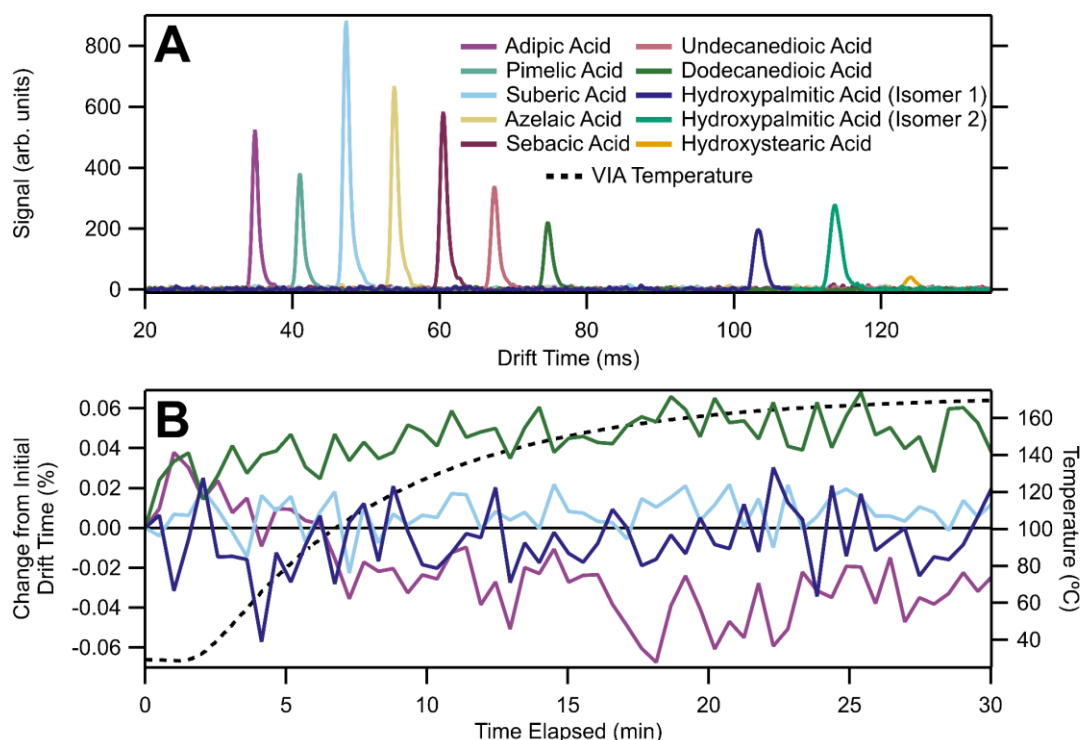
3.1 Carboxylic acid standards and instrument stability

Figure 1A shows the ion mobility spectrum of the 10 carboxylic acid standards using the VIA-CI-IMS-TOF with I⁻ reagent ions. Despite only one pair of isomers being included in this experiment (2- and 16-hydroxypalmitic acid), these standards serve as model compounds for demonstrating the separation ability and stability of the VIA-CI-IMS-TOF. The IMS parameters
170 used in the experiment were sufficient for baseline-resolved separation of each IMS peak. The resolution achieved in the IMS drift chamber is highly dependent on the pressure of the buffer gas (Deng et al., 2016) and thus it was hypothesized that the performance may be susceptible to large changes in temperature induced by the VIA installed in close proximity upstream. To evaluate the potential effects of heated sample air, the VIA temperature was increased from 30 °C to ~170 °C over a period of



30 min while sampling the standards from the chamber, and the drift times of each standard were monitored (Fig. 1B). It should be noted that, while thermal decomposition of analytes has been observed in the VIA (Zhao et al., 2024), the carboxylic acids used here exhibited sufficient thermal stability for this experiment and minor amounts of decomposition would not have impacted IMS separation.

Pressures within the CI-IMS-TOF, including the IMS drift region, were minimally affected by the changing VIA temperature. Although the AIM reactor pressure decreased slightly as the VIA exceeded 100 °C (Fig. S2), downstream effects were mitigated by the automatic pressure regulation in the IMS. The IMS drift region pressure remained within the required ± 4 μ bar tolerance despite trending inversely with VIA temperature (Fig. S3). Prior to performing the drift time calibration, IMS peak positions of the standards changed by up to $\sim 0.4\%$ in correlation with the drift region pressure (Figs. S4-5). After calibration, however, deviations in the drift times were largely mitigated, with most peaks remaining within 0.05% of their initial positions and the maximum deviation being only -0.075% (for 12-hydroxystearic acid). These shifts are at least ~ 20 times smaller than the width of individual peaks. The minor shifts in drift time after calibration did not appear to correlate with VIA temperature and differences between diacids and hydroxyacids were not discernible (Fig. S6). With the ability to minimize temperature-induced changes in drift time through calibration, the VIA-CI-IMS-TOF provides a useful platform to speciate isomers in aerosols and could reasonably be used for thermal ramping experiments.



190 **Figure 1: A) Calibrated ion mobility spectrum of 10 carboxylic acid standards and B) relative change from initial calibrated IMS drift time throughout VIA temperature ramping for adipic, suberic, dodecanedioic, hydroxypalmitic acids. While only a subset of standards is shown in panel B for clarity, the effects of the temperature ramping are representative of all tested standards.**

3.2 Environmental chamber experiment

195 Previous studies using IM-MS (Krechmer et al, 2016; Skyttä et al. 2022) and LC-ESI-HRMS (Kristensen et al., 2016, 2017;
Kenseth et al., 2020) has illustrated the isomeric complexity of the gas- and particle-phase compounds formed from α -pinene
ozonolysis. Multiple isomers were observed for several reaction products in these studies, including at least two for $C_9H_{14}O_4$
and as many as five for $C_{10}H_{16}O_4$. While many observed isomers were attributed by Skyttä et al. (2022) to cluster isomers (*i.e.*,
reagent ions bound to different sites of a single molecular structure), other literature on the analysis of α -pinene ozonolysis
products by IM-MS supports the presence of isomers for several molecular formulas (Krechmer et al., 2016; Zhang et al.,
200 2017; West et al., 2023). The formation of isomers is further supported by the generally accepted mechanisms of the reaction
of α -pinene with ozone and the OH radicals generated from the decomposition of Criegee intermediates (Aschmann et al.,
2003). A simplified view of these reactions is shown in Fig. 2, which includes two $C_8H_{12}O_4$ isomers (terpenylic and norpinic
acid), two $C_9H_{14}O_4$ isomers (*cis*-pinic acid and 4-hydroxypinalic-3-acid), and two other products discussed in this text (pinonic
and 10-hydroxypinonic acid). Given this complexity and the large body of literature that exists for this system, SOA generated
205 from the α -pinene ozonolysis reaction was chosen here to evaluate the performance of the VIA-CI-IMS-TOF.

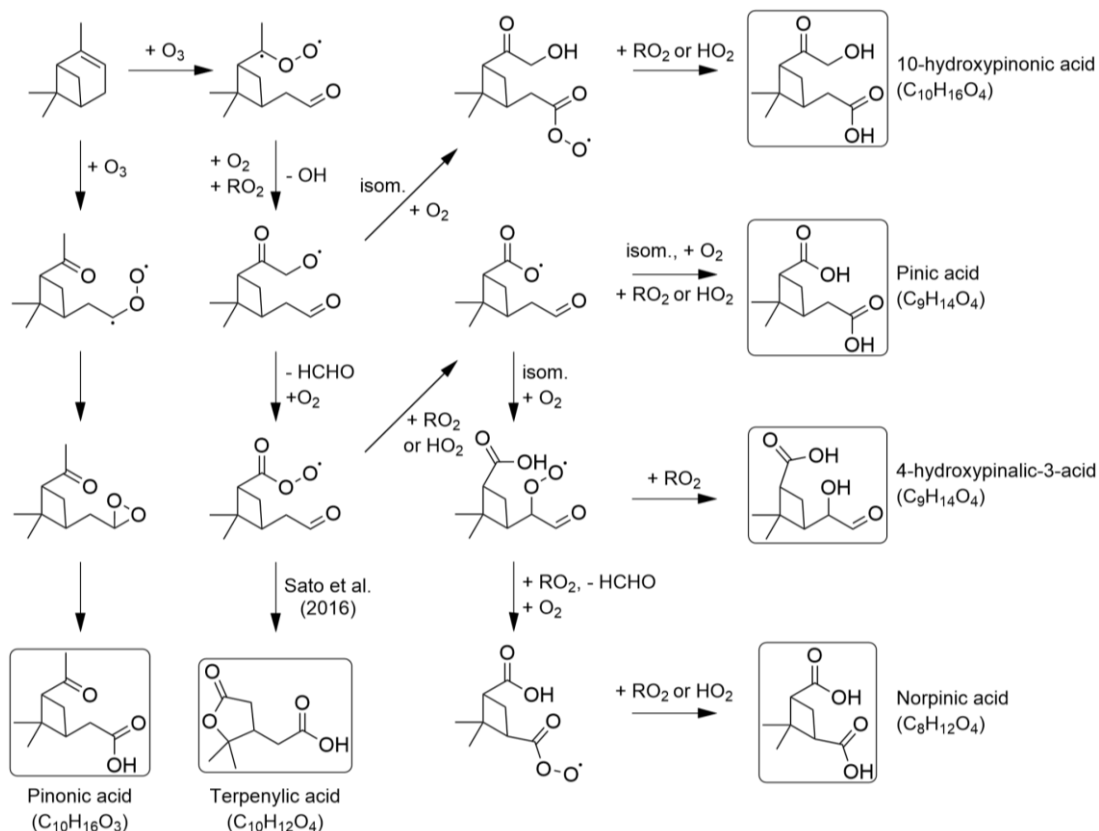


Figure 2. Simplified mechanism adapted from Ma et al. (2008) and Sato et al. (2016) for the formation of six products of α -pinene ozonolysis discussed in this text. For clarity, the final reaction steps in the formation of terpenylic acid proposed by Sato et al. (2016) have been omitted from this scheme.



210

Figure 3 shows the measured ion mobility spectra for $C_8H_{12}O_4$, $C_9H_{14}O_4$, $C_{10}H_{16}O_3$, and $C_{10}H_{16}O_4$ along with the spectra of the synthetic standards which share these formulas. Note that all ions were detected as clusters with I^- (or Br^-), but the formula of the neutral is used for simplicity everywhere in this paper. The spectra were averaged over a one-minute segment near the end of an α -pinene ozonolysis experiment with the exception of $C_{10}H_{16}O_3$ and its corresponding standard, which required an averaging period of 10 minutes to improve signal-to-noise ratios. Multiple isomers were observed for each molecular formula during the experiment and, using the ion mobility spectra obtained using the authentic standards, at least four compounds could be confidently identified.

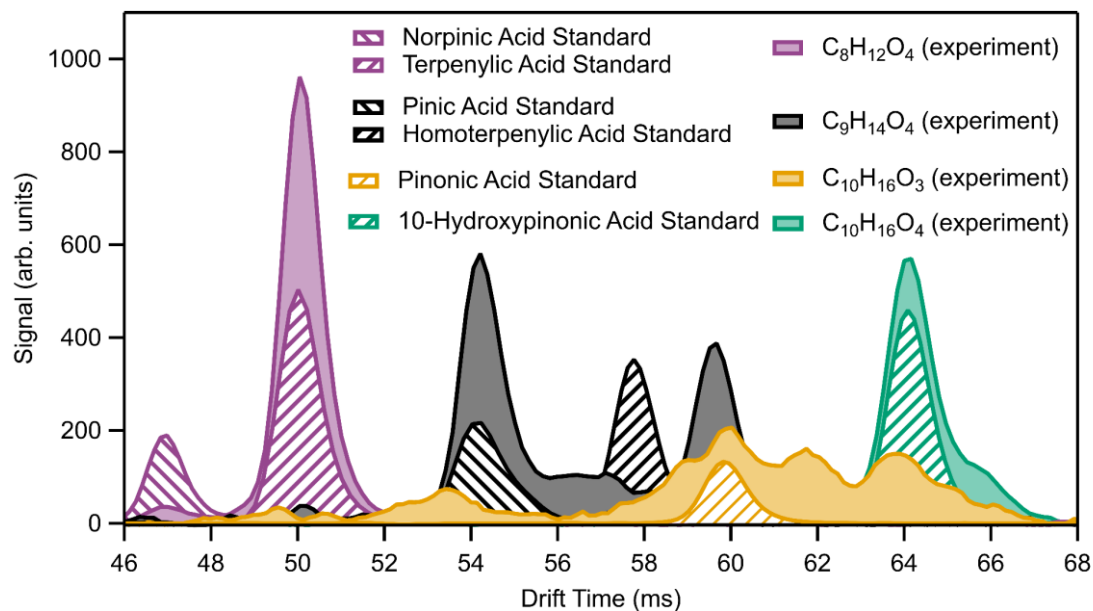
215

220

225

230

In Fig. 3, two peaks can be observed in the $C_8H_{12}O_4$ IMS spectrum, indicating the presence of two distinct isomers, both of which align with synthetic standards based on drift time and peak shape. The first of these isomers was identified as norpinic acid, a well-characterized product of α -pinene ozonolysis (Ma et al., 2008), at a drift time of 47 ms. The second, larger peak observed at 50 ms was concluded to be terpenylic acid, a compound previously identified as a potential tracer for α -pinene SOA (Claeys et al., 2009). The observed difference in signal intensity agrees with reported measurements of these products in chamber experiments, which show that the SOA mass fractions of terpenylic acid under similar reaction conditions are considerably larger (up to or exceeding an order of magnitude) than that of norpinic acid (Winterhalter et al., 2003; Claeys et al., 2009; Amin et al., 2013; Kenseth et al., 2020). Terpenylic acid has been reported to arise from both ozonolysis and photooxidation, though the proposed mechanisms for the ozonolysis pathway differ (Claeys et al., 2009; Sato et al., 2016). Most studies that have reported terpenylic acid as a product of α -pinene ozonolysis did not use an OH radical scavenger (Claeys et al., 2009; Yasmeen et al., 2010; Sato et al., 2016; Thomsen et al., 2022) or acknowledged low scavenging efficiency (Hatfield and Huff Hartz, 2011; Amin et al., 2013), leaving it ambiguous as to which oxidant primarily contributes to its formation. However, Kenseth et al. (2023) showed that the SOA mass fraction of terpenylic acid formed from α -pinene ozonolysis was minimally impacted by the use of an OH scavenger (>95% scavenging efficiency), suggesting that it is primarily a product of ozone-initiated reactions. Although determining the exact origin of terpenylic acid in this experiment was beyond the scope of this work, the VIA-CI-IMS-TOF could be a useful tool for clarifying this and other reaction pathways, particularly when used to monitor isomer populations in real time as discussed in later in this section.



235

Figure 3: Ion mobility spectrum of α -pinene ozonolysis products and six synthetic standards. Signals have been scaled for presentation on the same y-axis, but relative intensities within a single trace (e.g., $C_8H_{12}O_4$) are unchanged.

240

A more complex IMS spectrum was observed for $C_9H_{14}O_4$ (Fig. 3) during the α -pinene ozonolysis experiment, containing two prominent peaks and a region of unresolved signal between ~ 54 and 60 ms. The first IMS peak of $C_9H_{14}O_4$ (54.2 ms) was identified with a synthetic standard as *cis*-pinic acid, a commonly observed dicarboxylic acid product of α -pinene ozonolysis (Ma et al., 2008). Conversely, no resolved IMS peak was observed during the α -pinene ozonolysis experiment at the drift time of the homoterpenylic acid standard (57.8 ms). This is in agreement with Yasmeeen et al. (2010) and Mutzel et al. (2016), who identified homoterpenylic acid as a β -pinene SOA tracer compound and noted little to production of this compound from α -pinene ozonolysis. The structures of the unresolved $C_9H_{14}O_4$ signals and large peak near 60 ms were not determined here, though multiple isomers of this molecular formula have been reported in the literature (Ma et al., 2008; Skyttä et al., 2022). For example, Jaoui and Kamens (2003) tentatively identified a $C_9H_{14}O_4$ product of β -pinene ozonolysis as 4-hydroxypinonic-3-acid and, as later suggested by Ma et al. (2008), may also be present in α -pinene ozonolysis SOA. While an authentic standard for 4-hydroxypinonic-3-acid is not currently available, it may be possible to synthesize one for future experiments in order to better understand the chemical composition of this system.

250

At least five IMS peaks were observed for $C_{10}H_{16}O_3$ during the chamber experiment, though the weak signal poses a challenge for accurate peak identification. There was no definitive alignment of any of the $C_{10}H_{16}O_3$ peaks with that of the *cis*-pinonic acid standard, though it may be assigned as a tentative match with the largest peak at 60.2 ms. While *cis*-pinonic acid is a well-known product of α -pinene ozonolysis (Ma et al., 2007a), its relatively high volatility generally prevents substantial partitioning into the particle phase (Müller et al., 2012). Additionally, previous measurement of α -pinene ozonolysis SOA by LC-ESI-HRMS has shown it to be only a minor component of the total aerosol mass under reaction conditions similar to those

255



used in this study (Zhang et al., 2015; Kenseth et al., 2020). The small amount that may have been present in the SOA measured here could have been poorly detected by the CI-IMS-TOF due to the adduct declustering effects discussed below in section 3.3. There have been few reports of $C_{10}H_{16}O_3$ isomers other than pinonic acid in α -pinene ozonolysis SOA, which suggests that our data either represent previously undetected compounds or are possible sampling artifacts related to the VIA (e.g., thermal decomposition products, denuder inefficiency). Changing the temperature of the VIA and evaluating the efficiency of the charcoal denuder would help to clarify this in future experiments.

Lastly, at least two isomers of $C_{10}H_{16}O_4$ were observed during the chamber experiment, one of which was identified as 10-hydroxypinonic acid at a drift time of 64 ms. The ion mobility spectrum of $C_{10}H_{16}O_4$ from the chamber experiment is quite similar to the results obtained by Zhang et al. (2017), who used electrospray ionization and IM-MS for offline analysis of SOA generated through ozonolysis and photooxidation of α -pinene. Specifically, in the photooxidation-derived SOA, the ion mobility spectrum corresponding to the sodium adduct of $C_{10}H_{16}O_4$ shows a similar amount of isomeric complexity to that in Fig. 3, whereas the ozonolysis spectrum contains only a single prominent peak. Considering the high OH radical yield of α -pinene ozonolysis (Aschmann et al., 2003) and the lack of an OH scavenger in our experiment, the observation of reaction products from both reaction pathways is not surprising. It is also possible that the additional $C_{10}H_{16}O_4$ IMS peak corresponds to other isomers of hydroxypinonic acid, whether formed during the reaction (Kenseth et al., 2020) or from thermal decomposition of high molecular weight dimers in the VIA (Müller et al., 2008; Huang et al., 2018). While we did not investigate this possibility further, alterations to the chamber reaction conditions and varying the VIA temperature could assist in determining the origin of these species.

In addition to online identification of individual isomers of reaction products, the VIA-CI-IMS-TOF enables real-time monitoring of the temporal evolution of these isomers throughout the chamber experiment. Figure 4 shows the time series of total MS signal and individual isomer signal for $C_9H_{14}O_4$ and $C_{10}H_{16}O_4$, two molecular formulas for which multiple isomers were observed. In both cases, the inclusion of the IMS time series provides more information than the MS signal alone. This feature can be particularly helpful in chamber experiments designed to elucidate reaction mechanisms by distinguishing first-generation products from those generated later in a reaction.

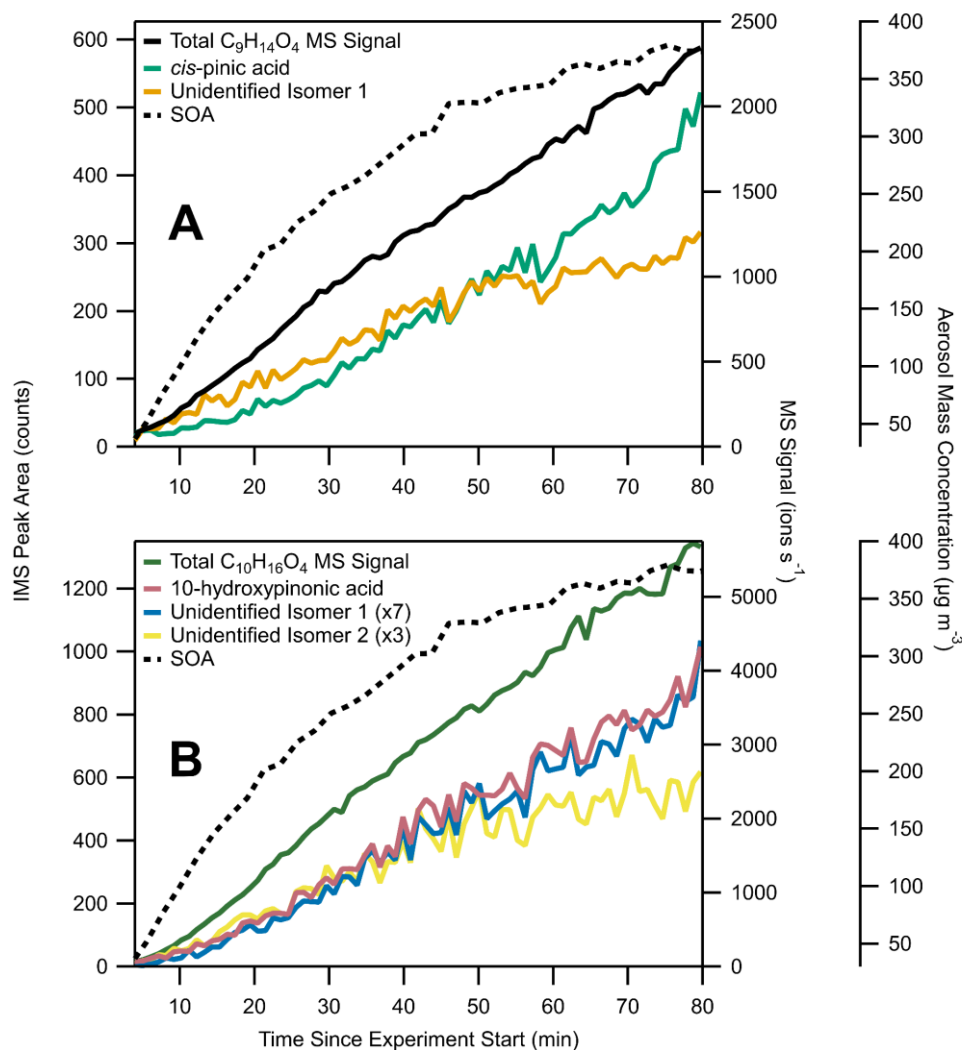


Figure 4: VIA-CI-TOF-MS time series of C₉H₁₄O₄ (panel A) and C₁₀H₁₆O₄ (panel B) and SMPS signal during the α -pinene ozonolysis experiment. The left and right y-axes correspond to the IMS peak areas and total MS signal, respectively, and the far right axis corresponds to the SMPS signal.

285 Distinct temporal behavior of isomers is particularly clear in Fig. 4A, in which the total MS signal for C₉H₁₄O₄ is approximately linear throughout the experiment, whereas the IMS time series for *cis*-pinic acid and an unidentified isomer display increasing and decreasing rates of growth, respectively. This difference can be explained in part by the influence of OH radicals throughout the experiment. In addition to being produced by ozonolysis (Ma et al., 2007b), *cis*-pinic acid can also be generated through the reactions of OH radicals with pinonic acid (Librando and Tringali, 2005) and α -pinene (Eddingsaas et al., 2012). Additionally, particle-phase formation of *cis*-pinic acid has also been proposed (Zhang et al., 2015; Kenseth et al., 2023) and may account for a portion of the observed signal, especially late in the experiment when most of the α -pinene had been consumed. Given the accelerating production of *cis*-pinic acid during the end of the experiment when most of the α -

290

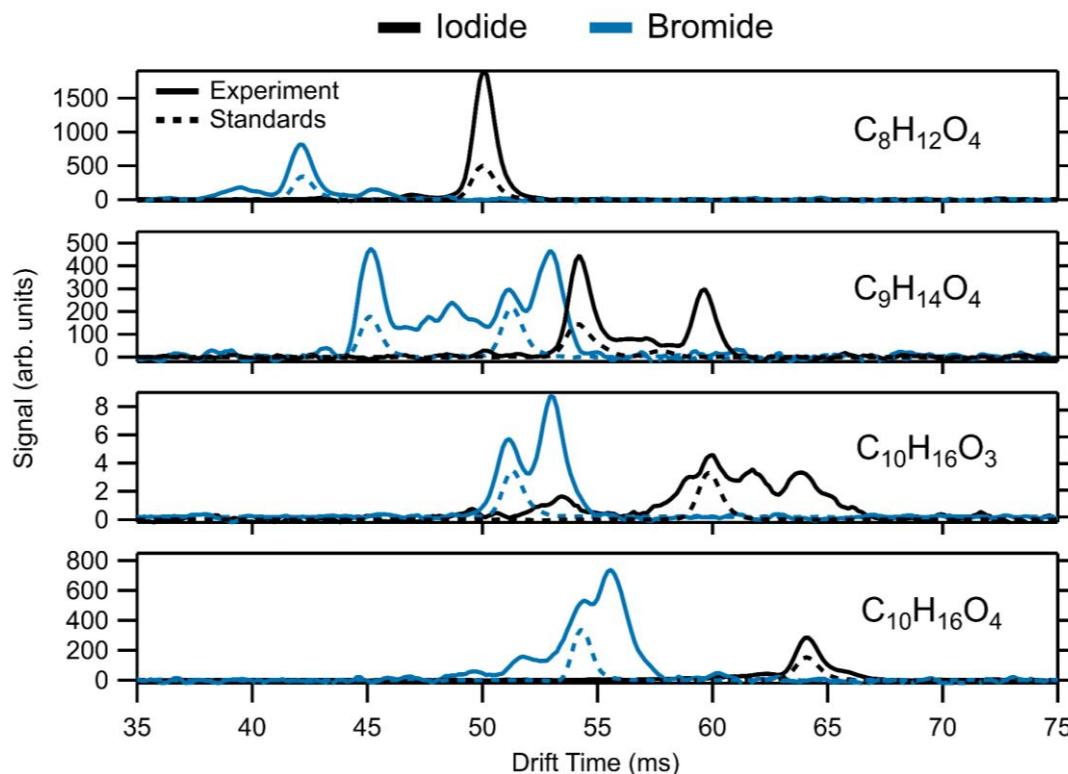


pinene had been consumed, second-generation chemistry (whether from pinonic acid photooxidation or particle-phase chemistry) is likely its dominant source. Production of the unidentified $C_9H_{14}O_4$ isomer, on the other hand, does not accelerate throughout the reaction, indicating that it is likely a first-generation product of α -pinene oxidation (Ma et al., 2008). While the identity of this species was not determined, multiple isomers of $C_9H_{14}O_4$ resulting from α -pinene ozonolysis (e.g., 4-hydroxypinonic-3-acid) and photooxidation have previously been reported (Ma et al., 2008; Skyttä et al., 2022).

Similar information can be gleaned from panel B of Fig. 4, which shows the total MS signal for $C_{10}H_{16}O_4$ as well as IMS time series for 10-hydroxypinonic acid and two unidentified isomers. First, it is clear that 10-hydroxypinonic acid accounts for the largest fraction of the total $C_{10}H_{16}O_4$ signal and also most closely resembles the overall time series with a linear time profile. While the structures of the other $C_{10}H_{16}O_4$ isomers are unclear, it is possible to gain some insight into their origins from their time series. During the reaction, the first unidentified isomer exhibited a linear growth rate after an initial delay period relative to the total $C_{10}H_{16}O_4$ signal, suggesting that this species was generated through a pathway other than direct ozonolysis that requires accumulation of primary reaction products. Growth of the second unidentified isomer, however, slowed near the end of the reaction and can be identified as a probable first-generation product of α -pinene oxidation.

3.3 Compatibility with Other Reagent Ions

Figure 5 shows the comparison of signals for several α -pinene ozonolysis reaction products when operating the VIA-CI-IMS-TOF with I^- and Br^- reagent ions. Despite similar detection selectivity between I^- and Br^- , the ion mobility spectra generated with each are notably different. Note that the ion mobility changes for the same species due to the different size of the reagent ions and the relative distributions of cluster geometries. The first difference between the spectra in Fig. 5 is a larger number of isomers detectable as Br^- adducts than as I^- adducts, with the exception of $C_{10}H_{16}O_3$, for which only two resolved peaks are visible as Br^- adducts compared to at least five when detected using I^- . This can be largely attributed to the differences in adduct binding energies between the two reagent ions and the stability of these adducts in the IMS drift region. A recent computational study showed that the gas-phase binding energy of Br^- with highly oxidized organic compounds tends to be higher than that of analogous I^- adducts at low humidities (Hytinen et al., 2018). In the case of the compounds shown in Fig. 5, these differences appear to be comparable to the amount of energy imparted to the ions during IMS separation, allowing some Br^- -analyte adducts to remain intact whereas the I^- analogues are declustered prior to reaching the TOF. It is also important to consider the differences in relative signal intensity between each set of IMS spectra, as the peaks that seem largest in one mode might not be the same in the other mode (e.g., $C_{10}H_{16}O_3$ in Fig. 5). In addition to only showing a limited view of how many isomers are present for a given molecular formula, using only one reagent ion provides a skewed view of relative abundances unless each isomer has been calibrated for using synthetic standards. Using the AIM reactor's ability to easily switch between multiple reagent ions (Riva et al., 2024), a more comprehensive characterization of the molecular composition of SOA can be performed.



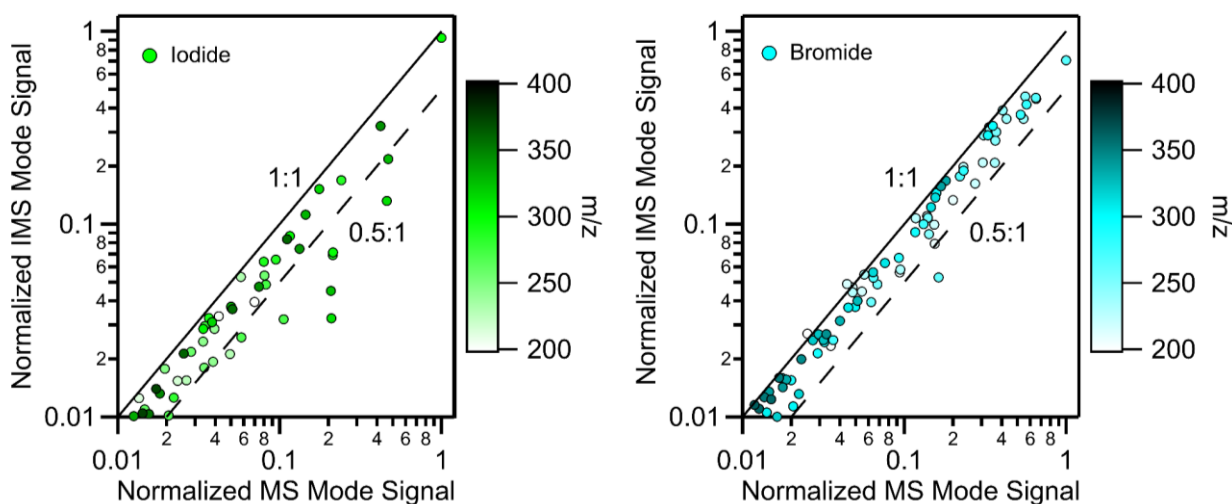
325 **Figure 5:** Ion mobility spectra of four chemical formulas clustered with I^- or Br^- ions observed during the α -pinene oxidation experiments. Data from the chamber experiments are displayed as solid lines and the synthetic standards are shown as dashed lines.

The CI-IMS-TOF can be operated in an MS-only mode that bypasses the IMS drift region or in IMS mode, in which the ion path is directed through the drift region. The use of IMS mode, however, comes at the expense of ion transmission through the instrument. Ion loss in the CI-IMS-TOF is largely driven by the 50% duty cycle of the ion gating sequence used to introduce discrete ions packets to the mobility region (Kamrath and Lopez-Hilfiker, 2023), and signal reduction exceeding 50% can be attributed to physical ion losses and the adduct declustering effect described above. If the ion gating sequence is used during both operating modes, thus applying the 50% duty cycle to both measurements, differences in ion-molecule adduct stability through the drift region can be more directly observed.

335 The loss of analyte signal due to IMS separation in the CI-IMS-TOF can be observed in Fig. 6, which shows unit mass resolution (UMR) signals of α -pinene ozonolysis products clustered with I^- and Br^- in IMS mode plotted against those acquired in MS-only mode. If no declustering or other signal losses occurred, all points would fall along the 1:1 line indicating equal signal strength in both modes. In general, Br^- adducts trended closer to the 1:1 line, suggesting appreciably stronger binding energies with α -pinene ozonolysis products than I^- , which exhibited a larger deviation from the 1:1 line and several signals falling below the 0.5:1 line. The differences in signal loss between the reagent ions can also be seen by comparing the mass spectra collected in both operating modes (Fig. S7). While some peaks in the mass spectra are depleted by only ~10-30% (e.g., m/z 299 in the I^- spectrum and m/z 335 in the Br^- spectrum), much higher signal losses were observed for others that



presumably form weakly bound adducts with the reagent ion. For example, the signal corresponding to $C_{10}H_{16}O_3I^-$ (m/z 311.015) was reduced by more than 90% relative to when it was measured in MS-only mode, which may explain the lack of a clear *cis*-pinonic acid signal in the ion mobility spectrum shown in Fig. 3. As shown in Fig. S7, the use of Br^- also enabled the detection of a larger number of reaction products and thereby allowed for the IMS separation of isomers that did not form strongly bound I^- adducts. In future applications of the VIA-CI-IMS-TOF, the use of multiple reagent ions including and in addition to I^- and Br^- could help to mitigate biases introduced by analyte-dependent ion loss and provide a more complete view of the reaction products formed in a chamber experiment.



350 **Figure 6:** Scatter plots of normalized UMR signals of α -pinene ozonolysis products clustered with I^- and Br^- measured in MS and IMS modes. The signals were averaged over ~ 1 minute near the end of the experiment and normalized to the highest signal in MS mode for each reagent ion. Isotopic peaks and peaks not clustered with I^- or Br^- (*i.e.*, signals with even m/z values) were removed for clarity.

4 Conclusions

355 We have demonstrated the feasibility of isomer-resolved analysis of organic aerosol in real time using the Aerodyne VIA coupled with IM-MS detection. The compatibility of the two components was evaluated by increasing the VIA temperature while continuously measuring 10 condensed-phase standards. Throughout a ~ 150 °C increase, the measured IMS drift times were found to be stable to within approximately 0.05% of their initial values, a change ~ 20 times smaller than the width of individual mobility peaks. The minimal impact of inlet temperature on IMS performance suggests that this method can be
360 further applied to environmental chamber experiments, including temperature ramping of the VIA to assess the volatility of SOA constituents.

The performance of the VIA-CI-IMS-TOF was assessed through online analysis of α -pinene ozonolysis and subsequent offline analysis of synthetic reaction product standards. Multiple distinct ion mobility peaks were observed for



several reaction products, corroborating the presence of structural isomers as reported previously for this system. Four
365 compounds – *cis*-norpinic acid, terpenylic acid, *cis*-pinic acid, and 10-hydroxypinonic acid – were confidently identified
through the use of synthetic standards. By comparing time series of pinic and OH-pinonic acids with other structural isomers
throughout the reaction, we showed the potential for this system to be used in conjunction with environmental chamber
experiments to gain insight into complex reaction mechanisms from the temporal evolution of reaction intermediates and
products.

370 Advantages of using multiple reagent ions in the VIA-CI-IMS-TOF for molecular characterization of SOA were also
shown through the comparison of ion mobility and mass spectra of α -pinene ozonolysis products detected with I^- and Br^- .
Despite the substantial overlap in the clustering selectivity of these ions, an increase in the number of IMS peaks and less
signal loss in the IMS were observed when the instrument was operated in Br^- mode. This observation is consistent with
stronger binding energies calculated for Br^- than I^- with oxygenated organic compounds and shows how multiple reagent ions
375 can be used to provide a more comprehensive characterization of organic aerosols.

This study provides a proof-of-concept demonstration of the VIA-CI-IMS-TOF system and demonstrates its use for
online, isomer-resolved analysis of organic aerosol. While the system performed well for the analysis of a high-concentration
chamber experiment, several improvements could be made to expand its range of applications. Operation of the CI-IMS-TOF,
including optimization of the IMS voltage parameters and further stabilization of the drift region pressure, could serve to
380 enhance overall sensitivity, IMS peak separation, and IMS peak resolution. Real-time analysis with the VIA-CI-IMS-TOF
could also be systematically applied to additional atmospherically relevant aerosols to better understand reaction mechanisms,
compound yields, or other phenomena that are challenging to study with offline methods or non-isomer resolved online
methods.

385 *Data availability.* Data for this work is available upon request. The figure files for this manuscript, including the data in
numerical form, can be downloaded from https://cires1.colorado.edu/jimenez/group_pubs.html.

Author Contributions. AFS and KHB conceptualized the project. JLJ and JAdG obtained the IMS instrument and training and
provided laboratory space and tools. HS developed the software used to analyze the CI-IMS-TOF data and improved it for our
390 analysis. AFS performed the chamber experiments and data analysis, generated the figures and tables, and wrote the paper.
CMK synthesized and provided the reaction product standards. MRC provided the VIA and assisted with experimental design.
MR provided input on IMS operation and data interpretation. All authors discussed the results and reviewed and edited the
paper.

395 *Competing Interests.* MRC and HS are employees of Aerodyne Research Inc., which sells the VIA and CI-IMS-TOF.



Financial Support. This research was partially supported by grants from the Balvi Philanthropic Fund (A29) and NSF (AGS-2206655). CMK acknowledges support from NSF (AGS-2132296).

References

- 400 Amarandei, C., Olariu, R. I., Arsene, C., Amarandei, C., Olariu, R. I., and Arsene, C.: Implications of Matrix Effects in Quantitative HPLC/ESI-ToF-MS Analyses of Atmospheric Organic Aerosols, *Proceedings*, 55, <https://doi.org/10.3390/proceedings2020055006>, 2020.
- Amin, H. S., Hatfield, M. L., and Huff Hartz, K. E.: Characterization of secondary organic aerosol generated from ozonolysis of α -pinene mixtures, *Atmos. Environ.*, 67, 323–330, <https://doi.org/10.1016/j.atmosenv.2012.10.063>, 2013.
- 405 Apffel, A., Fischer, S., Goldberg, G., Goodley, P. C., and Kuhlmann, F. E.: Enhanced sensitivity for peptide mapping with electrospray liquid chromatography-mass spectrometry in the presence of signal suppression due to trifluoroacetic acid-containing mobile phases, *J. Chromatogr. A*, 712, 177–190, [https://doi.org/10.1016/0021-9673\(95\)00175-M](https://doi.org/10.1016/0021-9673(95)00175-M), 1995.
- Aschmann, S. M., Tuazon, E. C., Arey, J., and Atkinson, R.: Products of the Gas-Phase Reaction of O₃ with Cyclohexene, *J. Phys. Chem. A*, 107, 2247–2255, <https://doi.org/10.1021/jp022122e>, 2003.
- 410 Bi, C., Krechmer, J. E., Frazier, G. O., Xu, W., Lambe, A. T., Clafin, M. S., Lerner, B. M., Jayne, J. T., Worsnop, D. R., Canagaratna, M. R., and Isaacman-Vanwertz, G.: Coupling a gas chromatograph simultaneously to a flame ionization detector and chemical ionization mass spectrometer for isomer-resolved measurements of particle-phase organic compounds, *Atmospheric Meas. Tech.*, 14, 3895–3907, <https://doi.org/10.5194/amt-14-3895-2021>, 2021a.
- Bi, C., Krechmer, J. E., Frazier, G. O., Xu, W., Lambe, A. T., Clafin, M. S., Lerner, B. M., Jayne, J. T., Worsnop, D. R., Canagaratna, M. R., and Isaacman-Vanwertz, G.: Quantification of isomer-resolved iodide chemical ionization mass spectrometry sensitivity and uncertainty using a voltage-scanning approach, *Atmospheric Meas. Tech.*, 14, 6835–6850, <https://doi.org/10.5194/amt-14-6835-2021>, 2021b.
- Bilde, M., Barsanti, K., Booth, M., Cappa, C. D., Donahue, N. M., Emanuelsson, E. U., McFiggans, G., Krieger, U. K., Marcolli, C., Topping, D., Ziemann, P., Barley, M., Clegg, S., Dennis-Smith, B., Hallquist, M., Hallquist, Å. M., Khlystov, A., Kulmala, M., Mogensen, D., Percival, C. J., Pope, F., Reid, J. P., Silva, M. A. V. R. D., Rosenoern, T., Salo, K., Soonsin, V. P., Yli-Juuti, T., Prisle, N. L., Pagels, J., Rarey, J., Zardini, A. A., and Riipinen, I.: Saturation Vapor Pressures and Transition Enthalpies of Low-Volatility Organic Molecules of Atmospheric Relevance: From Dicarboxylic Acids to Complex Mixtures, *Chem. Rev.*, 115, 4115–4156, <https://doi.org/10.1021/cr5005502>, 2015.
- 420 Chen, X., Kangasluoma, J., Kubečka, J., Neeffjes, I., Vehkamäki, H., Kulmala, M., Tootchi, A., Mubas Sirah, F., Hua, L., Larríba-Andaluz, C., and Junninen, H.: On the dependence of electrical mobility on temperature, humidity and structure of alkylammonium ions, *J. Aerosol Sci.*, 179, 106353, <https://doi.org/10.1016/j.jaerosci.2024.106353>, 2024.
- Claeys, M., Inuma, Y., Szmigielski, R., Surratt, J. D., Blockhuys, F., Alsenoy, C. V., Böge, O., Sierau, B., Gómez-González, Y., Vermeylen, R., Veken, P. V. D., Shahgholi, M., Chan, A. W. H., Herrmann, H., Seinfeld, J. H., and Maenhaut, W.:



- 430 Terpenylic acid and related compounds from the oxidation of α -pinene: Implications for new particle formation and growth above forests, *Environ. Sci. Technol.*, 43, 6976–6982, <https://doi.org/10.1021/es9007596>, 2009.
- Deng, L., Ibrahim, Y. M., Hamid, A. M., Garimella, S. V. B., Webb, I. K., Zheng, X., Prost, S. A., Sandoval, J. A., Norheim, R. V., Anderson, G. A., Tolmachev, A. V., Baker, E. S., and Smith, R. D.: Ultra-High Resolution Ion Mobility Separations Utilizing Traveling Waves in a 13 m Serpentine Path Length Structures for Lossless Ion Manipulations Module, *Anal. Chem.*, 88, 8957–8964, <https://doi.org/10.1021/acs.analchem.6b01915>, 2016.
- 435 Donahue, N. M., Drozd, G. T., Epstein, S. A., Presto, A. A., and Kroll, J. H.: Adventures in ozoneland: down the rabbit-hole, *Phys. Chem. Chem. Phys.*, 13, 10848–10857, <https://doi.org/10.1039/C0CP02564J>, 2011.
- Eatough, D. J., Long, R. W., Modey, W. K., and Eatough, N. L.: Semi-volatile secondary organic aerosol in urban atmospheres: meeting a measurement challenge, *Atmos. Environ.*, 37, 1277–1292, [https://doi.org/10.1016/S1352-2310\(02\)01020-8](https://doi.org/10.1016/S1352-2310(02)01020-8), 2003.
- 440 Eddingsaas, N. C., Loza, C. L., Yee, L. D., Seinfeld, J. H., and Wennberg, P. O.: α -pinene photooxidation under controlled chemical conditions – Part 1: Gas-phase composition in low- and high-NO_x environments, *Atmospheric Chem. Phys.*, 12, 6489–6504, <https://doi.org/10.5194/acp-12-6489-2012>, 2012.
- Finewax, Z., Jimenez, J. L., and Ziemann, P. J.: Development and application of a low-cost vaporizer for rapid, quantitative, in situ addition of organic gases and particles to an environmental chamber, *Aerosol Sci. Technol.*, 54, 1567–1578, <https://doi.org/10.1080/02786826.2020.1808186>, 2020.
- 445 Hatfield, M. L. and Huff Hartz, K. E.: Secondary organic aerosol from biogenic volatile organic compound mixtures, *Atmos. Environ.*, 45, 2211–2219, <https://doi.org/10.1016/j.atmosenv.2011.01.065>, 2011.
- Hallquist, M., Wenger, J. C., Baltensperger, U., Rudich, Y., Simpson, D., Claeys, M., Dommen, J., Donahue, N. M., George, C., Goldstein, A. H., Hamilton, J. F., Herrmann, H., Hoffmann, T., Iinuma, Y., Jang, M., Jenkin, M. E., Jimenez, J. L., Kiendler-Scharr, A., Maenhaut, W., McFiggans, G., Mentel, T. F., Monod, A., Prévôt, A. S. H., Seinfeld, J. H., Surratt, J. D., Szmigielski, R., and Wildt, J.: The formation, properties and impact of secondary organic aerosol: current and emerging issues, *Atmospheric Chem. Phys.*, 9, 5155–5236, <https://doi.org/10.5194/acp-9-5155-2009>, 2009.
- 450 Hildmann, S. and Hoffmann, T.: Characterisation of atmospheric organic aerosols with one- and multidimensional liquid chromatography and mass spectrometry: State of the art and future perspectives, *TrAC Trends Anal. Chem.*, 175, 117698, <https://doi.org/10.1016/j.trac.2024.117698>, 2024.
- 455 Huang, W., Saathoff, H., Pajunoja, A., Shen, X., Naumann, K.-H., Wagner, R., Virtanen, A., Leisner, T., and Mohr, C.: α -Pinene secondary organic aerosol at low temperature: chemical composition and implications for particle viscosity, *Atmospheric Chem. Phys.*, 18, 2883–2898, <https://doi.org/10.5194/acp-18-2883-2018>, 2018.
- Hyttinen, N., Otkjær, R. V., Iyer, S., Kjaergaard, H. G., Rissanen, M. P., Wennberg, P. O., and Kurtén, T.: Computational Comparison of Different Reagent Ions in the Chemical Ionization of Oxidized Multifunctional Compounds, *J. Phys. Chem. A*, 122, 269–279, <https://doi.org/10.1021/acs.jpca.7b10015>, 2018.
- 460



- Jaoui, M. and Kamens, R. M.: Mass Balance of Gaseous and Particulate Products from β -Pinene/O₃/Air in the Absence of Light and β -Pinene/NO_x/Air in the Presence of Natural Sunlight, *J. Atmospheric Chem.*, 45, 101–141, <https://doi.org/10.1023/A:1024093710794>, 2003.
- 465 Kamrath, M. and Lopez-Hilfiker, F.: Isomer Separation with Vocus Ion Mobility Spectrometry, TOFWERK, Switzerland, 2023.
- Kenseth, C. M., Hafeman, N. J., Huang, Y., Dalleska, N. F., Stoltz, B. M., and Seinfeld, J. H.: Synthesis of Carboxylic Acid and Dimer Ester Surrogates to Constrain the Abundance and Distribution of Molecular Products in α -Pinene and β -Pinene Secondary Organic Aerosol, *Environ. Sci. Technol.*, 54, 12829–12839, <https://doi.org/10.1021/acs.est.0c01566>, 2020.
- 470 Kenseth, C. M., Hafeman, N. J., Rezgui, S. P., Chen, J., Huang, Y., Dalleska, N. F., Kjaergaard, H. G., Stoltz, B. M., Seinfeld, J. H., and Wennberg, P. O.: Particle-phase accretion forms dimer esters in pinene secondary organic aerosol, *Science*, 787–792, <https://doi.org/10.1126/science.adi0857>, 2023.
- Kenseth, C. M.; Hakan, O. L.; Dalleska, N. F.; Lalic, G.; Stoltz, B. M.; Seinfeld, J. H.; Thornton, J. A. Synthesis of Molecular Products in Pinene Secondary Organic Aerosol. *Environ. Sci. Technol. Lett.*, In Preparation.
- 475 Krechmer, J. E., Groessl, M., Zhang, X., Junninen, H., Massoli, P., Lambe, A. T., Kimmel, J. R., Cubison, M. J., Graf, S., Lin, Y. H., Budisulistiorini, S. H., Zhang, H., Surratt, J. D., Knochenmuss, R., Jayne, J. T., Worsnop, D. R., Jimenez, J. L., and Canagaratna, M. R.: Ion mobility spectrometry-mass spectrometry (IM-MS) for on- and offline analysis of atmospheric gas and aerosol species, *Atmospheric Meas. Tech.*, 9, 3245–3262, <https://doi.org/10.5194/amt-9-3245-2016>, 2016.
- 480 Krechmer, J. E., Pagonis, D., Ziemann, P. J., and Jimenez, J. L.: Quantification of gas-wall partitioning in teflon environmental chambers using rapid bursts of low-volatility oxidized species generated in situ, *Environ. Sci. Technol.*, 50, 5757–5765, <https://doi.org/10.1021/acs.est.6b00606>, 2016.
- Krechmer, J. E., Day, D. A., Ziemann, P. J., and Jimenez, J. L.: Direct measurements of gas/particle partitioning and mass accommodation coefficients in environmental chambers, *Environ. Sci. Technol.*, 51, 11867–11875, <https://doi.org/10.1021/acs.est.7b02144>, 2017.
- 485 Kristensen, K., Watne, K. A., Hammes, J., Lutz, A., Petäjä, T., Hallquist, M., Bilde, M., and Glasius, M.: High-molecular weight dimer esters are major products in aerosols from α -pinene ozonolysis and the boreal forest, *Environ. Sci. Technol. Lett.*, 3, 280–285, <https://doi.org/10.1021/acs.estlett.6b00152>, 2016
- Kristensen, K., Jensen, L. N., Glasius, M., and Bilde, M.: The effect of sub-zero temperature on the formation and composition of secondary organic aerosol from ozonolysis of alpha-pinene, *Environ. Sci.: Processes Impacts*, 19, 1220–1234, <https://doi.org/10.1039/C7EM00231A>, 2017
- 490 Law, W. S., Wang, R., Hu, B., Berchtold, C., Meier, L., Chen, H., and Zenobi, R.: On the Mechanism of Extractive Electrospray Ionization, *Anal. Chem.*, 82, 4494–4500, <https://doi.org/10.1021/ac100390t>, 2010.
- Librando, V. and Tringali, G.: Atmospheric fate of OH initiated oxidation of terpenes. Reaction mechanism of α -pinene degradation and secondary organic aerosol formation, *J. Environ. Manage.*, 75, 275–282, <https://doi.org/10.1016/j.jenvman.2005.01.001>, 2005.



- 495 Lopez-Hilfiker, F. D., Mohr, C., Ehn, M., Rubach, F., Kleist, E., Wildt, J., Mentel, Th. F., Lutz, A., Hallquist, M., Worsnop, D., and Thornton, J. A.: A novel method for online analysis of gas and particle composition: description and evaluation of a Filter Inlet for Gases and AEROsols (FIGAERO), *Atmos. Meas. Tech.*, 7, 983–1001, <https://doi.org/10.5194/amt-7-983-2014>, 2014.
- Ma, Y., Luciani, T., Porter, R. A., Russell, A. T., Johnson, D., and Marston, G.: Organic acid formation in the gas-phase ozonolysis of α -pinene, *Phys. Chem. Chem. Phys.*, 9, 5084–5087, <https://doi.org/10.1039/b709880d>, 2007a.
- 500 Ma, Y., Willcox, T. R., Russell, A. T., and Marston, G.: Pinic and pinonic acid formation in the reaction of ozone with α -pinene, *Chem. Commun.*, 1328–1330, <https://doi.org/10.1039/b617130c>, 2007b.
- Ma, Y., Russell, A. T., and Marston, G.: Mechanisms for the formation of secondary organic aerosol components from the gas-phase ozonolysis of α -pinene, *Phys. Chem. Chem. Phys.*, 10, 4294, <https://doi.org/10.1039/b803283a>, 2008.
- 505 Miljevic, B., Hedayat, F., Stevanovic, S., Fairfull-Smith, K. E., Bottle, S. E., and Ristovski, Z. D.: To Sonicate or Not to Sonicate PM Filters: Reactive Oxygen Species Generation Upon Ultrasonic Irradiation, *Aerosol Sci. Technol.*, 48, 1276–1284, <https://doi.org/10.1080/02786826.2014.981330>, 2014.
- Morris, M. A., Pagonis, D., Day, D. A., de Gouw, J. A., Ziemann, P. J., and Jimenez, J. L.: Absorption of volatile organic compounds (VOCs) by polymer tubing: implications for indoor air and use as a simple gas-phase volatility separation technique, *Atmos. Meas. Tech.*, 17, 1545–1559, <https://doi.org/10.5194/amt-17-1545-2024>, 2024.
- 510 Müller, L., Reinnig, M.-C., Warnke, J., and Hoffmann, T.: Unambiguous identification of esters as oligomers in secondary organic aerosol formed from cyclohexene and cyclohexene/ α -pinene ozonolysis, *Atmospheric Chem. Phys.*, 8, 1423–1433, <https://doi.org/10.5194/acp-8-1423-2008>, 2008.
- Müller, L., Reinnig, M.-C., Naumann, K. H., Saathoff, H., Mentel, T. F., Donahue, N. M., and Hoffmann, T.: Formation of 3-methyl-1,2,3-butanetricarboxylic acid via gas phase oxidation of pinonic acid – a mass spectrometric study of SOA aging, *Atmospheric Chem. Phys.*, 12, 1483–1496, <https://doi.org/10.5194/acp-12-1483-2012>, 2012.
- Mutzel, A., Rodigast, M., Iinuma, Y., Böge, O., and Herrmann, H.: Monoterpene SOA – Contribution of first-generation oxidation products to formation and chemical composition, *Atmos. Environ.*, 130, 136–144, <https://doi.org/10.1016/j.atmosenv.2015.10.080>, 2016.
- 520 Peng, Z. and Jimenez, J.L.: KinSim: a research-grade, user-friendly, visual kinetics simulator for chemical-kinetics and environmental-chemistry teaching, *J. Chem. Educ.*, 96, 806–811, <https://doi.org/10.1021/acs.jchemed.9b00033>, 2019.
- Pöschl, U.: Atmospheric Aerosols: Composition, Transformation, Climate and Health Effects, *Angew. Chem. Int. Ed.*, 44, 7520–7540, <https://doi.org/10.1002/anie.200501122>, 2005.
- Presto, A. A. and Donahue, N. M.: Ozonolysis fragment quenching by nitrate formation: the pressure dependence of prompt OH radical formation, *J. Phys. Chem. A*, 108, 9096–9104, <https://doi.org/10.1021/jp047162s>, 2004.
- 525 Resch, J., Wolfer, K., Barth, A., and Kalberer, M.: Effects of storage conditions on the molecular-level composition of organic aerosol particles, *Atmospheric Chem. Phys.*, 23, 9161–9171, <https://doi.org/10.5194/acp-23-9161-2023>, 2023.



- Rice, R. L., Riva, M., Mettke, P., Iyer, S., Gerber, S., Graf, S., Lopez-Hilfiker, F., Kamrath, M., Zhang, Z., Herrmann, H., Surratt, J. D., and Gold, A.: Hydroxyl radical-initiated oxidation of isoprene leads to a cyclic peroxyhemiacetal via 1,6-hydrogen shift chemistry that yields secondary organic aerosol, *Environ. Sci. Technol.*, 60, 3374–3383, <https://doi.org/10.1021/acs.est.5c09701>, 2026.
- Riva, M., Pospisilova, V., Frege, C., Perrier, S., Bansal, P., Jorga, S., Sturm, P., Thornton, J. A., Rohner, U., and Lopez-Hilfiker, F.: Evaluation of a reduced-pressure chemical ion reactor utilizing adduct ionization for the detection of gaseous organic and inorganic species, *Atmospheric Meas. Tech.*, 17, 5887–5901, <https://doi.org/10.5194/amt-17-5887-2024>, 2024.
- Sato, K., Jia, T., Tanabe, K., Morino, Y., Kajii, Y., and Imamura, T.: Terpenylic acid and nine-carbon multifunctional compounds formed during the aging of β -pinene ozonolysis secondary organic aerosol, *Atmos. Environ.*, 130, 127–135, <https://doi.org/10.1016/j.atmosenv.2015.08.047>, 2016.
- Schaum, A. F., Bates, K. H., Min, K.-E., Myers, F., Longnecker, E. R., Canagaratna, M. R., Alton, M. W., and Ziemann, P. J.: A simple, versatile approach for coupling a liquid chromatograph and chemical ionization mass spectrometer for offline analysis of organic aerosol, *Aerosol Res.*, 3, 557–568, <https://doi.org/10.5194/ar-3-557-2025>, 2025.
- Shilling, J. E., Chen, Q., King, S. M., Rosenoern, T., Kroll, J. H., Worsnop, D. R., DeCarlo, P. F., Aiken, A. C., Sueper, D., Jimenez, J. L., and Martin, S. T.: Loading-dependent elemental composition of α -pinene SOA particles, *Atmos. Chem. Phys.*, 9, 771–782, <https://doi.org/10.5194/acp-9-771-2009>, 2009.
- Shrivastava, M., Cappa, C. D., Fan, J., Goldstein, A. H., Guenther, A. B., Jimenez, J. L., Kuang, C., Laskin, A., Martin, S. T., Ng, N. L., Petaja, T., Pierce, J. R., Rasch, P. J., Roldin, P., Seinfeld, J. H., Shilling, J., Smith, J. N., Thornton, J. A., Volkamer, R., Wang, J., Worsnop, D. R., Zaveri, R. A., Zelenyuk, A., and Zhang, Q.: Recent advances in understanding secondary organic aerosol: Implications for global climate forcing, *Rev. Geophys.*, 55, 509–559, <https://doi.org/10.1002/2016RG000540>, 2017.
- Skyttä, A., Gao, J., Cai, R., Ehn, M., Ahonen, L. R., Kurten, T., Wang, Z., Rissanen, M. P., and Kangasluoma, J.: Isomer-Resolved Mobility-Mass Analysis of α -Pinene Ozonolysis Products, *J. Phys. Chem. A*, 126, 5040–5049, <https://doi.org/10.1021/acs.jpca.2c03366>, 2022.
- Stark, H., Yatavelli, R. L. N., Thompson, S. L., Kimmel, J. R., Cubison, M. J., Chhabra, P. S., Canagaratna, M. R., Jayne, J. T., Worsnop, D. R., and Jimenez, J. L.: Methods to extract molecular and bulk chemical information from series of complex mass spectra with limited mass resolution, *Int. J. Mass Spectrom.*, 389, 26–38, 2015.
- Taylor, P. J.: Matrix effects: the Achilles heel of quantitative high-performance liquid chromatography–electrospray–tandem mass spectrometry, *Clin. Biochem.*, 38, 328–334, <https://doi.org/10.1016/j.clinbiochem.2004.11.007>, 2005.
- Thomsen, D., Thomsen, L. D., Iversen, E. M., Björgvinsdóttir, T. N., Vinther, S. F., Skønager, J. T., Hoffmann, T., Elm, J., Bilde, M., and Glasius, M.: Ozonolysis of α -Pinene and Δ^3 -Carene Mixtures: Formation of Dimers with Two Precursors, *Environ. Sci. Technol.*, 56, 16643–16651, <https://doi.org/10.1021/acs.est.2c04786>, 2022.
- Tobias, H. J. and Ziemann, P. J.: Thermal desorption mass spectrometric analysis of organic aerosol formed from reactions of 1-tetradecene and O_3 in the presence of alcohols and carboxylic acids, *Environ. Sci. Technol.* 34, 2105–2115, <https://doi.org/10.1021/es9907156>, 2000.



- Verevkin, S. P., Kozlova, S. A., Emel'yanenko, V. N., Nikitin, E. D., Popov, A. P., and Krasnykh, E. L.: Vapor Pressures, Enthalpies of Vaporization, and Critical Parameters of a Series of Linear Aliphatic Dimethyl Esters of Dicarboxylic Acids, *J. Chem. Eng. Data*, 51, 1896–1905, <https://doi.org/10.1021/je0602418>, 2006.
- 565 West, C. P., Mesa Sanchez, D., Morales, A. C., Hsu, Y.-J., Ryan, J., Darmody, A., Slipchenko, L. V., Laskin, J., and Laskin, A.: Molecular and Structural Characterization of Isomeric Compounds in Atmospheric Organic Aerosol Using Ion Mobility-Mass Spectrometry, *J. Phys. Chem. A*, 127, 1656–1674, <https://doi.org/10.1021/acs.jpca.2c06459>, 2023.
- Williams, B. J., Goldstein, A. H., Kreisberg, N. M., and Hering, S. V.: An in-situ instrument for speciated organic composition of atmospheric aerosols: thermal desorption aerosol GC/MS-FID (TAG), *Aerosol Sci. Technol.*, 40, 627–638, <https://doi.org/10.1080/02786820600754631>, 2006.
- 570 Winterhalter, R., Van Dingenen, R., Larsen, B. R., Jensen, N. R., and Hjorth, J.: LC-MS analysis of aerosol particles from the oxidation of α -pinene by ozone and OH-radicals, *Atmospheric Chem. Phys. Discuss.*, 3, 1–39, <https://doi.org/10.5194/acpd-3-1-2003>, 2003.
- Yasmeen, F., Vermeulen, R., Szmigielski, R., Iinuma, Y., Böge, O., Herrmann, H., Maenhaut, W., and Claeys, M.: Terpenylic acid and related compounds: precursors for dimers in secondary organic aerosol from the ozonolysis of α - and β -pinene, *Atmospheric Chem. Phys.*, 10, 9383–9392, <https://doi.org/10.5194/acp-10-9383-2010>, 2010.
- 575 Zhang, Q., Jimenez, J. L., Canagaratna, M. R., Allan, J. D., Coe, H., Ulbrich, I., Alfarra, M. R., Takami, A., Middlebrook, A. M., Sun, Y. L., Dzepina, K., Dunlea, E., Docherty, K., DeCarlo, P. F., Salcedo, D., Onasch, T., Jayne, J. T., Miyoshi, T., Shimono, A., Hatakeyama, S., Takegawa, N., Kondo, Y., Schneider, J., Drewnick, F., Borrmann, S., Weimer, S., Demerjian, K., Williams, P., Bower, K., Bahreini, R., Cottrell, L., Griffin, R. J., Rautiainen, J., Sun, J. Y., Zhang, Y. M., and Worsnop, D. R., Ubiquity and dominance of oxygenated species in organic aerosols in anthropogenically-influenced Northern Hemisphere midlatitudes, *Geophys. Res. Lett.*, 34, L13801, <https://doi.org/10.1029/2007GL029979>, 2007.
- 580 Zhang, X., McVay, R. C., Huang, D. D., Dalleska, N. F., Aumont, B., Flagan, R. C., and Seinfeld, J. H.: Formation and evolution of molecular products in α -pinene secondary organic aerosol, *Proc. Natl. Acad. Sci.*, 112, 14168–14173, <https://doi.org/10.1073/pnas.1517742112>, 2015.
- 585 Zhang, X., Lambe, A. T., Upshur, M. A., Brooks, W. A., Bé, A. G., Thomson, R. J., Geiger, F. M., Surratt, J. D., Zhang, Z., Gold, A., Graf, S., Cubison, M. J., Groessl, M., Jayne, J. T., Worsnop, D. R., and Canagaratna, M. R.: Highly Oxygenated Multifunctional Compounds in α -Pinene Secondary Organic Aerosol, *Environ. Sci. Technol.*, 51, 5932–5940, <https://doi.org/10.1021/acs.est.6b06588>, 2017.
- 590 Zhang, X., Zhang, H., Xu, W., Wu, X., Tyndall, G. S., Orlando, J. J., Jayne, J. T., Worsnop, D. R., and Canagaratna, M. R.: Molecular characterization of alkyl nitrates in atmospheric aerosols by ion mobility mass spectrometry, *Atmospheric Meas. Tech.*, 12, 5535–5545, <https://doi.org/10.5194/amt-12-5535-2019>, 2019.
- Zhao, J., Mickwitz, V., Luo, Y., Häkkinen, E., Graeffe, F., Zhang, J., Timonen, H., Canagaratna, M., Krechmer, J. E., Zhang, Q., Kulmala, M., Kangasluoma, J., Worsnop, D., and Ehn, M.: Characterization of the Vaporization Inlet for Aerosols (VIA)



595 for online measurements of particulate highly oxygenated organic molecules (HOMs), *Atmospheric Meas. Tech.*, 17, 1527–1543, <https://doi.org/10.5194/amt-17-1527-2024>, 2024.